ELSEVIER

Journal of Orthopaedic Research 23 (2005) 663–670

Journal of Orthopaedic Research

www.elsevier.com/locate/orthres

Mechanobiology of mandibular distraction osteogenesis: finite element analyses with a rat model

Elizabeth G. Loboa [a,*], Tony D. Fang [b], David W. Parker [a], Stephen M. Warren [b], Kenton D. Fong [b], Michael T. Longaker [b], Dennis R. Carter [a]

[a] *Biomechanical Engineering Division, Mechanical Engineering Department, Stanford University, Stanford, CA 94305, USA*
[b] *Department of Surgery, Stanford University School of Medicine, Stanford University, Stanford, CA 94305, USA*

Accepted 28 September 2004

Abstract

Three-dimensional finite element (FE) analyses were performed to characterize the local mechanical environment created within the tissue regenerate during mandibular distraction osteogenesis (DO) in a rat model. Finite element models were created from three-dimensional computed tomography image data of rat hemi-mandibles at four different time points during an optimal distraction osteogenesis protocol (i.e., most successful protocol for bone formation): end latency (post-operative day (POD) 5), distraction day 2 (POD 7), distraction day 5 (POD 10), and distraction day 8 (POD 13). A 0.25 mm distraction was simulated and the resulting hydrostatic stresses and maximum principal tensile strains were determined within the tissue regenerate. When compared to previous histological findings, finite element analyses showed that tensile strains up to 13% corresponded to regions of new bone formation and regions of periosteal hydrostatic pressure with magnitudes less than 17 kPa corresponded to locations of cartilage formation. Tensile strains within the center of the gap were much higher, leading us to conclude that tissue damage would occur there if the tissue was not compliant enough to withstand such high strains, and that this damage would trigger formation of new mesenchymal tissue. These data were consistent with histological evidence showing mesenchymal tissue present in the center of the gap throughout distraction. Finite element analyses performed at different time points during distraction were instrumental in determining the changes in hydrostatic stress and tensile strain fields throughout distraction, providing a mechanical environment rationale for the different levels of bone formation in end latency, and distraction day 2, 5, and 8 specimens.

Keywords: Mechanobiology; Mandibular distraction osteogenesis; Finite element analysis; Computed tomography; Mesenchymal tissue differentiation

Introduction

Mandibular distraction osteogenesis (DO) is often a more complicated procedure than long bone lengthening [6]. This is due to the complex three-dimensional distraction necessary to alter both the size and shape of a mandible, as compared to the primarily unidirectional lengthening of a long bone [6]. Therefore, investigations into pre-operative computer planning, finite element (FE) modeling, and mathematical modeling of mandibles and mandibular DO have greatly escalated as researchers attempt to better determine, in a noninvasive manner, the most appropriate mandibular DO procedure for each patient prior to initiating surgery.

Previous investigators have studied pre-operative planning techniques for mandibular DO using computer

* Corresponding author. Address: Joint Department of Biomedical Engineering at UNC—Chapel Hill and NC State University, North Carolina State University, 433 Daniels Hall, Campus Box 7115, Raleigh, NC 27695, USA. Tel.: +1 919 513 4015; fax: +1 919 513 3814.
E-mail address: egloboa@ncsu.edu (E.G. Loboa).

0736-0266/$ - see front matter
doi:10.1016/j.orthres.2004.09.010

models [6,7,19], stereolithographic models [5], and three-dimensional physical models [20]. Mathematical models of mandibular DO have also been developed in attempts to determine the optimum distraction rate [21] and distraction vector [22] for the procedure. While all of these approaches are of interest in pre-operative planning, none of them can address the local tissue-level stresses and strains experienced by the multipotent mesenchymal tissue within the distraction gap, information that needs to be obtained in order to elucidate the local stresses and strains that lead to the highest amount of bone regeneration.

Using a two-dimensional, axisymmetric, idealized FE model of the distraction gap and osteotomized bone ends in a mouse tibia, investigators in our laboratory looked at patterns of hydrostatic stress and maximum principal tensile strain occurring within the regenerate tissue during long bone lengthening. They correlated these regions of stress and strain to patterns of tissue differentiation as predicted with a mechanobiological tissue differentiation concept (Fig. 1) [1]. They showed that bone formation corresponded to regions of mild hydrostatic stress and tensile strain and cartilage formation to regions of hydrostatic pressure. They also hypothesized that regions of hydrostatic tension accelerated bone regeneration [1]. However, that FE model consisted of an idealized geometry of the distracted specimen and the FE analysis was performed at only one time point during the distraction osteogenesis procedure.

In this study, we use a CT/FEA approach to analyze mandibular DO at four time points during the distraction procedure: end latency (POD 5), distraction day 2 (POD 7), distraction day 5 (POD 10), and distraction day 8 (POD 13). Our goal was to further expand and elucidate upon previous rat mandibular DO experimental findings where we determined that global tissue-level strains in the range of 10–12.5% provided a high rate of bone regeneration in a rat model of mandibular DO [9]. In that study, we performed a uniaxial analysis and

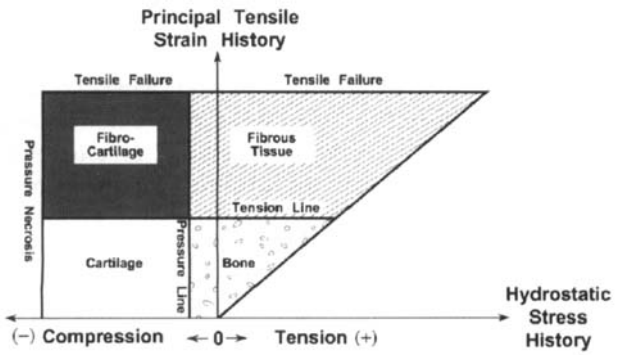

Fig. 1. Phase diagram of tissue differentiation concept relating mechanical loading history of multipotent mesenchymal tissue to skeletal tissue formation [1,3]. Tensile failure line marks cut-off region beyond which failure of tissue occurs and new mesenchymal tissue forms in response to tissue trauma [3,8,9].

determined the global tensile forces, stresses, and strains associated with distraction. However, we did not obtain information about hydrostatic stresses or about the local tissue-level tensile stresses and strains. In this follow-up study, we expanded upon our previous data with a three-dimensional finite element analysis of the distracted hemi-mandible in order to determine both the local tissue-level strains and the hydrostatic stresses resulting from distraction; and, we correlated this information with histological findings of bone and cartilage regeneration. To accomplish this, we used CT image data to create three-dimensional FE models of the distraction gap for specimens at the end of latency (POD 5), distraction day 2 (POD 7), distraction day 5 (POD 10), and distraction day 8 (POD 13). We simulated the application of a 0.25 mm displacement to each model, consistent with our previous experimental analyses [9] and an optimal in vivo distraction protocol [10], and calculated hydrostatic stresses and maximum principal tensile strains occurring throughout the tissue regenerate during distraction. Our research questions were: (1) What are the local hydrostatic stresses and tensile strains occurring within the multipotent mesenchymal tissue regenerate during mandibular DO; and, (2) do the patterns of hydrostatic stress and maximum principal tensile strain correspond to expected locations of bone regeneration, cartilage formation, and new mesenchymal tissue regeneration as we would predict with a mechanobiological tissue differentiation concept (Fig. 1) [1,3,8] and as we would expect given our previous experimental findings [9]?

Methods

Surgery and distraction protocol

All experiments were performed in accordance with Stanford University Animal Care and Use Committee Guidelines. Fifteen adult male Sprague–Dawley rats underwent surgery as previously described [9,18]. In brief, an incision was made over the right hemi-mandible, the masseter muscle was divided and the mandible exposed. An osteotomy was performed between the 2nd and 3rd molars and the resulting kerf was measured. Two Flexi-post pins were placed 4 mm anterior and posterior to the osteotomy, and a custom-made distraction device was fixed to the pins. The distraction protocol was described in our prior experimental study [9] and was the same as a previously published protocol for successful bone formation following mandibular distraction in a rat model [10]. This protocol was chosen because it provided optimal results for successful osteogenesis when compared to many other experimental protocols [10]. The protocol consisted of a 5-day latency period after the initial osteotomy followed by 8 days of distraction (0.25 mm distraction performed twice daily) followed by 28 days of maturation/consolidation when no distraction was applied.

Computed tomography (CT) imaging and creation of initial graphics exchange systems (IGES) surfaces

Harvested distraction gaps from end latency (POD 5), distraction day 2 (POD 7), distraction day 5 (POD 10), and distraction day 8 (POD 13) rat mandibles were imaged by three-dimensional CT (Model

CT/i, General Electric) with a voxel size of $0.187 \times 0.187 \times 1.00$ mm. We scanned the mandibles in air using axial mode at a voltage of 120 kV (peak) and a current of 150 mA. The smallest permissible scan field of view of 25 cm and display field of view of 9.6 cm were implemented and 1 mm slices were taken along the longitudinal/sagittal axis of the hemi-mandible.

A solid model of the tissue was constructed from the CT image data using a nonuniform rational B-spline (NURB) surface representation. Tissue centerlines were first obtained using the method described by Paik et al. [11]. A solid model of the regenerate tissue was created from both the centerlines and the CT image data using software described in Parker et al. [12]. In brief, a set of two-dimensional slice probes (geometrically defined as a rectangle imbedded in three-dimensional space) were positioned along the centerlines either by using a uniform sampling resolution or by a curvature measure. Each slice probe was oriented perpendicular to the centerline at its sampled position. Once the slice probes were defined and their size (width and height of the rectangle) specified, they were used to extract two-dimensional slices of data, each slice represented as a set of triangles, from the CT image data. Segmentation of the tissue for each two-dimensional data slice was performed using thresholding to create a set of profiles. Thresholding was performed by extracting an isocontour for a specified threshold level from the set of slice triangles. For each triangle in the slice, with CT intensity values $(c1, c2, c3)$ at the vertices, it was determined if the isocontour passed through the triangle by checking if the specified isocontour level c was within the intensity values for each triangle edge: $(c1, c2)$, $(c2, c3)$, and $(c3, c1)$. If it was, then its location on each edge, $x1$ and $x2$, was computed. The contour crossings $(x1, x2)$ for all the triangles were then combined to form a closed set of points, the profile, for a slice. The profiles were each fitted with a NURB curve. A NURB surface was then created by lofting the set of curves and capping the ends to create a solid model (Fig. 2). Isosurfaces extracted from the CT image data were compared to the solid model to ensure that the solid model accurately represented the desired tissue region, i.e., the region of regenerate tissue (Fig. 2). This process was repeated until solid models for end latency (POD 5), distraction day 2 (POD 7), distraction day 5 (POD 10), and distraction day 8 (POD 13) specimens were completed.

Solid models for all four specimens were imported into SolidWorks (SolidWorks Corporation, Concord, MA) and converted into IGES surfaces. The IGES surface for each specimen was then read into TrueGrid (v. 2.1.2, XYZ Scientific Applications, Livermore, CA, USA) for mesh creation.

Finite element modeling

In our previous experimental analyses, we performed mechanical testing on three specimens at each time point (end latency, distraction days 2, 5, and 8; total $n = 12$ for these time points) and calculated the average distraction gap, new bone formation, tensile stresses, and tensile strains at each time point for all the specimens [9]. To create our finite element models for the present study, we used CT data of the one specimen from each time point that most closely approximated the average dimensions for all three specimens at that time point. To ensure that the osteotomy gap was consistent with the average osteotomy gap determined from measurements taken at each surgery, osteotomized cortical bone segments within each model were approximated by rectangular cross sections centered within the surrounding multipotent mesenchymal tissue. New bone formation at each time point was modeled as two equal layers of new bone on each osteotomy end that progressed inward toward the center of the distraction gap. The thickness of these layers was determined from prior quantitative analysis of the histologies by (1) calculating the percent new bone formation within the distraction gap for each specimen ($n = 3$ at each time point) and (2) determining the average percent new bone formation for all three specimens at each time point [9]. The average percent new bone formation at each time point was implemented in the FE model for each time point.

End latency specimen

A three-dimensional finite element model of the end latency (POD 5) specimen was created in TrueGrid using 57,105 linear hexahedral elements comprised of 61,824 nodes. The geometry of the model was created using CT image data as described above. Cortical bone segments extended longitudinally from each end of the model into the center of the model and allowed for a 0.77 mm osteotomy gap within the 4.36 mm specimen (Fig. 3A). The value of 0.77 mm was obtained from kerf measurements obtained at surgery. The multipotent mesenchymal tissue regenerate was assumed to be homogeneous, isotropic, and nearly incompressible, was modeled as a linear elastic material, and was assigned an elastic modulus (E) of 0.05 MPa [13] and Poisson's ratio (ν) of 0.49 [1]. Cortical bone was assumed to be homogeneous and isotropic and was also modeled as a linear elastic material with $E = 14{,}250$ MPa and $\nu = 0.39$ (value calculated from equation $\nu = 0.5\ (\nu_{12} + \nu_{21})$ using other investigators' reported values of $\nu_{12} = 0.46$ and $\nu_{21} = 0.31$ (1 = longitudinal; 2 = transverse)) [2].

Distraction day 2 specimen

A three-dimensional model of the distraction day 2 (POD 7) specimen was created using TrueGrid and consisted of 28,517 linear hexahedral elements comprised of 31,532 nodes. All tissues were assumed to be homogeneous and isotropic and modeled as linear elastic materials. The average distraction gap after two days of distraction equaled 1.61 mm (initial 0.77 mm osteotomy gap + 0.84 mm average distraction) [9]. However, by distraction day 2, there was an average of $8.3 \pm .09\%$ new bone formation within this gap (Fig. 4B) [9]. Therefore, this model consisted of a region of original, osteotomized cortical bone extending longitudinally into the gap ($E = 14{,}250$ MPa, $\nu = 0.39$) [2], followed by new, 2-day-old bone extending farther into the gap ($E = 317$ MPa, $\nu = 0.49$), surrounded by multipotent mesenchymal tissue ($E = 0.05$ MPa [13], $\nu = 0.49$ [1]) (Fig. 3B). Material property values for new bone were calculated based on information from fracture healing where it has been shown that 90 days is the minimum length of time for full fracture healing to occur in adults [17]. Therefore, we assumed a 90-day length of time for multipotent mesenchymal tissue to fully differentiate into cortical bone and, using linear interpolation, calculated changes in material property values for regenerating bone on a daily basis. In this case, the distraction gap was comprised only of multipotent mesenchymal tissue at end latency (POD 5). Therefore, the new bone in the gap for distraction day 2 (POD 7) was a maximum of 2 days old. We calculated E and ν for the 2-day-old bone

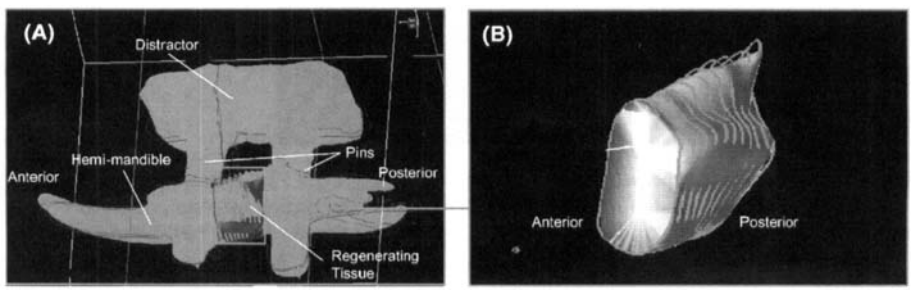

Fig. 2. Nonuniform rational B-spline (NURB) curves within the distraction gap are splined together and ends are capped to create a solid model (right) of regenerate tissue within the distraction gap.

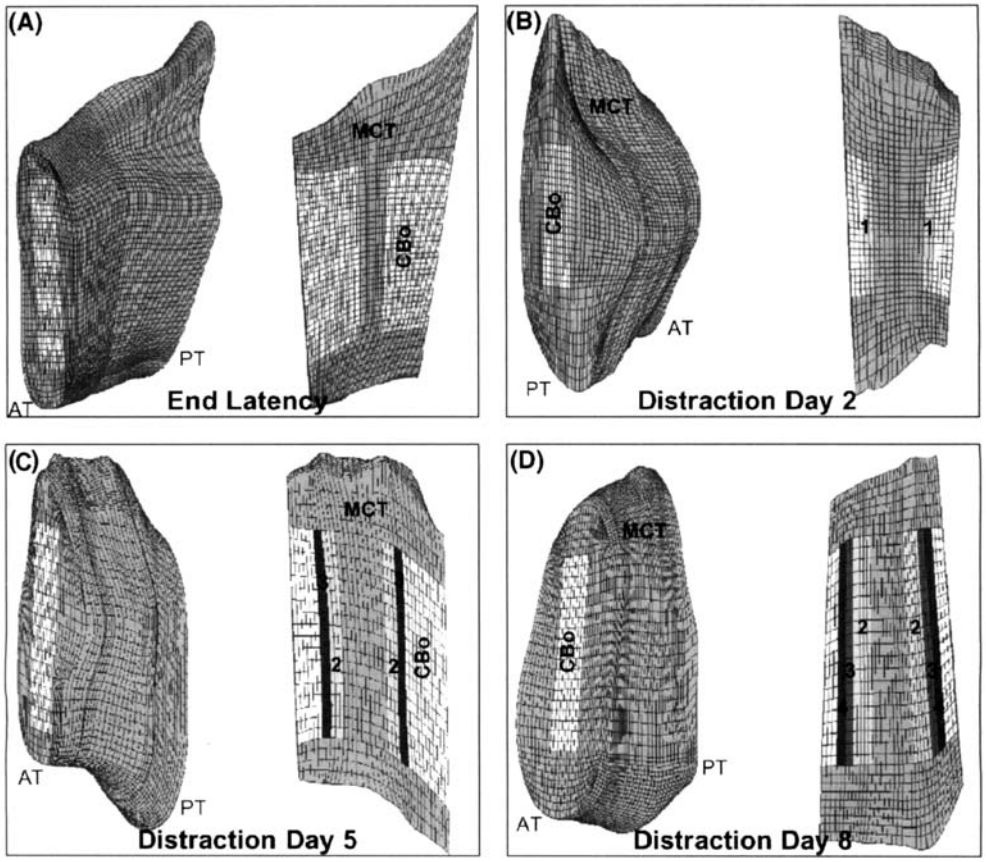

Fig. 3. Finite element models of specimens at various time points during distraction. A = end latency (post-operative day (POD) 5), B = distraction day 2 (POD 7), C = distraction day 5 (POD 10), and D = distraction day 8 (POD 13). Oblique view of the full three-dimensional model is shown on the left for each specimen and sagittal cut through the center of each model is shown on the right. CBo (white) = cortical bone; MCT = mesenchymal tissue; "1" = 2-day-old bone; "2" = 3-day-old bone; "3" = 5-day-old bone; "4" = 8-day-old bone. A 0.25 mm distraction was simulated by fixing one end of the specimen and simulating a sagittally oriented tensile displacement of 0.25 mm to the other end. AT = anterior; PT = posterior.

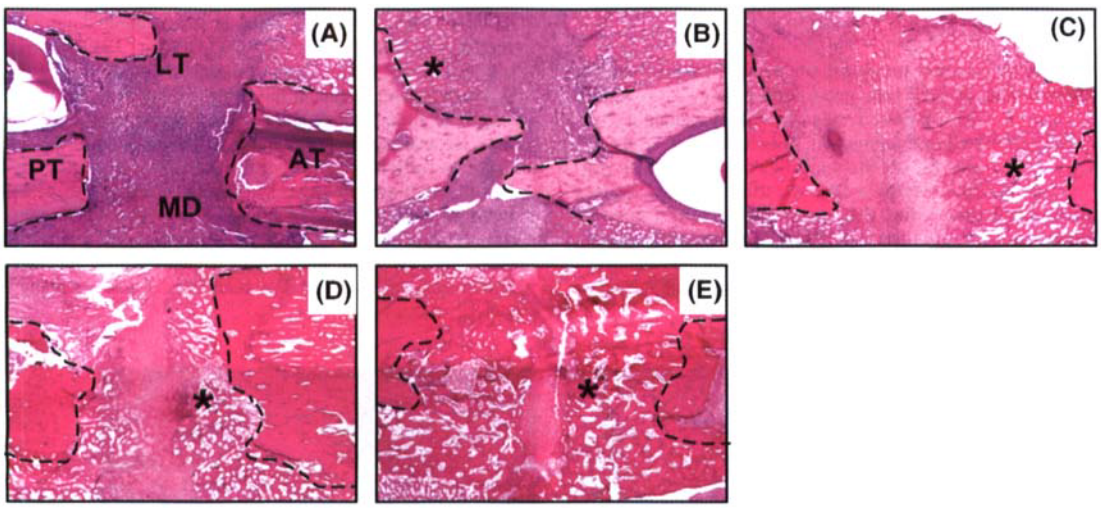

Fig. 4. Hematoxylin and Eosin of the distraction specimens (20×). A = end of latency (POD 5); B = distraction day 2 (POD 7); C = distraction day 5 (POD 10); D = distraction day 8 (POD 13); E = end of maturation (POD 41, end of distraction osteogenesis protocol when distractor is removed). AT = anterior, PT = posterior, LT = lateral, MD = medial. Dotted lines represent osteotomy fronts; (*) shows new trabecular bone.

by calculating the change from $E = 0.05$ MPa (mesenchymal tissue) [13] to $E = 14{,}250$ MPa (cortical bone) [2] and $\nu = 0.49$ (mesenchymal tissue) [1] to $\nu = 0.39$ (cortical bone) [2] over a 90-day period and, using linear interpolation, determined material properties of regenerating bone for each time point in between to arrive at $E = 317$ MPa and $\nu = 0.49$ for 2-day-old bone.

Distraction day 5 specimen

A three-dimensional model of the distraction day 5 (POD 10) specimen was created using TrueGrid and consisted of 25,012 linear hexahedral elements comprised of 27,702 nodes. All tissues were assumed to be homogeneous and isotropic and modeled as linear elastic materials. The average distraction gap after five days of distraction is equal to 2.87 mm (initial 0.77 mm osteotomy gap + 2.10 mm average distraction) [9]. However, by distraction day 5, there was an average of 31.6 ± 9.8% new bone formation within this gap (Fig. 4C) [9]. Therefore, this model consisted of a region of original, osteotomized cortical bone extending longitudinally into the gap (E = 14,250 MPa, ν = 0.39) [2], 5-day-old bone extending farther into the gap (E = 792 MPa, ν = 0.48), followed by 3-day-old bone extending farthest into the gap (E = 475 MPa, ν = 0.49), all surrounded by multipotent mesenchymal tissue (E = 0.05 MPa [13], ν = 0.49 [1]) (Fig. 3C). Material property values for new bone were calculated as described in *distraction day 2 specimen* above.

Distraction day 8 specimen

A three-dimensional model of the distraction day 8 (POD 13) specimen was created using TrueGrid and consisted of 31,212 linear hexahedral elements comprised of 34,300 nodes. All tissues were assumed to be homogeneous and isotropic and modeled as linear elastic materials. The average distraction gap after eight days of distraction was equal to 4.13 mm (initial 0.77 mm osteotomy gap + 3.36 mm distraction) [9]. However, by distraction day 8, there was an average of 54.9 ± 11.7% new bone formation within this gap (Fig. 4D) [9]. Therefore, this model consisted of a region of original, osteotomized cortical bone extending longitudinally into the gap (E = 14,250 MPa, ν = 0.39) [2], 8-day-old bone extending farther into the gap (E = 1267 MPa, ν = 0.48), 5-day-old bone extending even farther into the gap (E = 792 MPa, ν = 0.48), followed by 3-day-old bone extending farthest into the gap (E = 475 MPa, ν = 0.49), all surrounded by multipotent mesenchymal tissue (E = 0.05 MPa, ν = 0.49) (Fig. 3D). Material property values for new bone were calculated as described in *distraction day 2 specimen* above.

Finite element analyses

Once all of the three-dimensional meshes were created in TrueGrid, TrueGrid's Abaqus output option was used to create input files for solution using Abaqus (v. 5.8) software (Hibbitt, Karlsson and Sorensen, Inc., Pawtucket, RI, USA). We simulated a 0.25 mm distraction by fixing one end of the specimen and simulating a sagittally oriented tensile displacement of 0.25 mm to the other end (Fig. 3). The Abaqus finite element program was used to calculate hydrostatic stresses and tensile strains within the multipotent mesenchymal tissue regenerate of the distraction gap using a linear solver. MSC/PATRAN (v. 2000 r2) software (MSC Software Corp., Santa Ana, CA, USA) was used for post-processing of results.

Results

Hydrostatic stresses

Review of the hydrostatic stress plots for all specimens (Fig. 5) revealed that hydrostatic stresses were generally mild with the highest magnitudes of tensile hydrostatic stress below 97 kPa (9.69×10^{-2} MPa, experienced by distraction day 8 specimen, Fig. 5D). The highest magnitudes of tensile hydrostatic stress usually occurred in the distraction gap with all specimens also exhibiting some small periosteal regions of hydrostatic pressure (shown in white). The end latency (Fig. 5A) and distraction day 8 (Fig. 5D) specimens exhibited the highest levels of hydrostatic pressure with maximum pressures of 16.9 kPa and 8.5 kPa, respectively, as compared to the distraction day 2 (Fig. 5B) and distraction day 5 (Fig. 5C) specimens that had maximum hydrostatic pressures of 2.0 kPa and 8.3 kPa, respectively.

Maximum principal tensile strains

Review of the maximum principal tensile strain plots for all specimens (Fig. 6) revealed that tensile strains

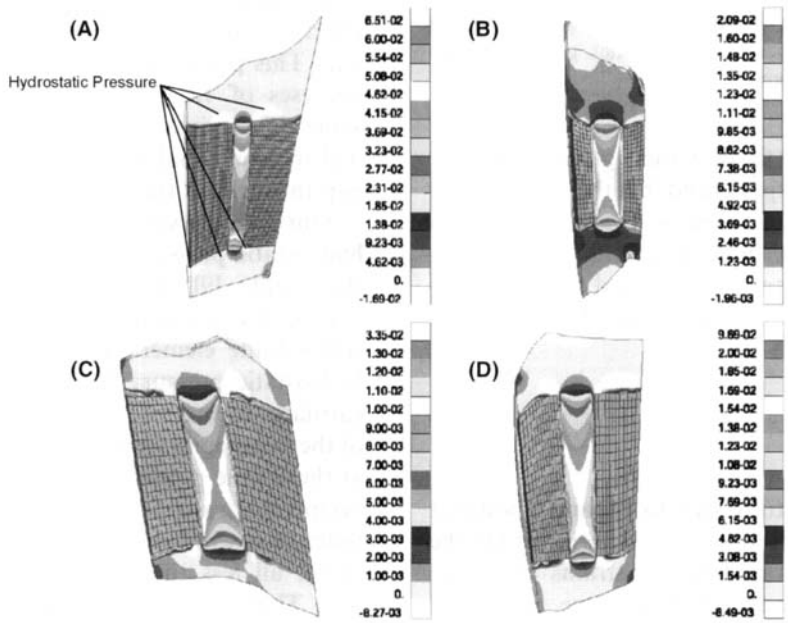

Fig. 5. Hydrostatic stresses (MPa) within mesenchymal tissue of: (A) end latency (POD 5) specimen; (B) distraction day 2 (POD 7) specimen; (C) distraction day 5 (POD 10) specimen; and, (D) distraction day 8 (POD 13) specimen. White periosteal areas show regions of hydrostatic pressure (negative hydrostatic stress). (A) fully labeled to clarify regions of hydrostatic pressure; (B)–(D) not labeled, hydrostatic pressure in white as shown in (A).

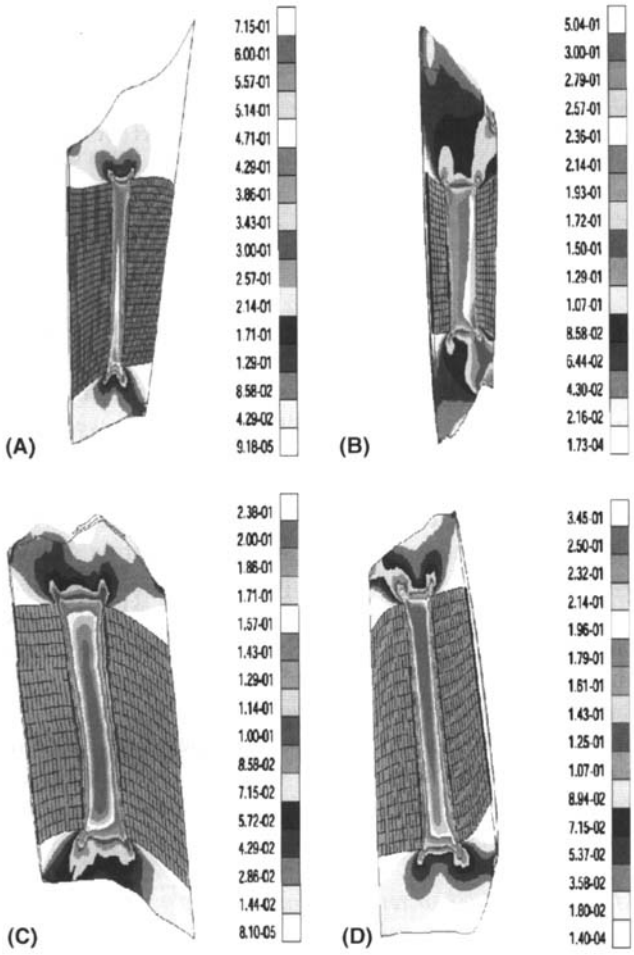

Fig. 6. Maximum principal tensile strains (mm/mm) within mesenchymal tissue of: (A) end latency (POD 5) specimen; (B) distraction day 2 (POD 7) specimen; (C) distraction day 5 (POD 10) specimen; and, (D) distraction day 8 (POD 13) specimen. In general, highest tensile strains occur in the center of the distraction gap with strains decreasing closer to the osteotomy ends.

within the mesenchymal tissue varied greatly with the highest tensile strains experienced by the end latency specimen (Fig. 6A) and the lowest by the distraction day 5 specimen (Fig. 6C). In general, strains were highest in the center of the distraction gap and decreased closer to the osteotomy ends and outside the distraction gap.

Discussion

The purpose of this study was to expand upon our previous experimental findings [9] to determine: (1) the local hydrostatic stresses and tensile strains occurring within the multipotent mesenchymal tissue regenerate during mandibular DO; and, (2) if the patterns of hydrostatic stress and maximum principal tensile strain corresponded to expected locations of bone regeneration, cartilage formation, and new mesenchymal tissue regeneration as predicted with a mechanobiological tissue differentiation concept (Fig. 1) [1,3,8].

Finite element results showed that maximum principal tensile strains up to 13% allowed for direct bone formation when hydrostatic stresses were mild (less than 97 kPa). These strains were consistent with those determined empirically where we found that global tensile strains in the range of approximately 10–12.5% appeared to accelerate bone regeneration [9]. Strain levels less than 13% were limited to specific regions of mesenchymal tissue at the ends of the osteotomy and periosteal to the osteotomized bone. While the end latency specimen (POD 5) experienced these levels of strains periosteally, almost no distraction gap strains were within this range (Fig. 6). The distraction day 2, 5, and 8 specimens, however, had larger regions within the distraction gap that exhibited strains in this range (Fig. 6). Therefore, as expected, the distraction day 2, 5, and 8 specimens exhibited a higher amount of bone formation in the distraction gap than the end latency specimen (Fig. 4B–D). These new findings were consistent with our previous empirical findings [9].

With our finite element analyses, we wanted to explore how the local tissue-level strains varied within the distraction gap, information that we could not determine with the uniaxial approach we took in our experimental study [9]. We found that, in general, strains were highest in the center of the distraction gap and decreased closer to the bone ends and outside the distraction gap (Fig. 6). Therefore, if tissue damage were to occur (i.e., if the tissue was not compliant enough to withstand such high strains), we expected this to happen in the center of the distraction gap [8]. As a result, new mesenchymal tissue regeneration would occur in the center of the gap. This prediction was supported by our histological analyses of 12 gradually distracted specimens at the same time points ($n = 3$ at each time point) that exhibited mesenchymal tissue in the center of the distraction gap throughout the distraction process (Fig. 4A–D) [9].

Our prior experimental analysis did not address hydrostatic pressure given the uniaxial assumptions for that study [9]. Therefore, we wanted to investigate hydrostatic pressure patterns with these three-dimensional finite element analyses. We expected regions of hydrostatic pressure to be consistent with locations of cartilage formation (Figs. 1 and 5) [3,1,8]. A review of the histologies from 12 gradually distracted specimens at these time points confirmed that cartilage formation occurred periosteally (Fig. 4) [9]. However, the magnitudes of hydrostatic pressure calculated here were quite small, all less than -17 kPa (-1.69×10^{-2} MPa, Fig. 5A). Thus, in some instances, we expected that periosteal bone may have formed instead of cartilage given an appropriate vascular supply (Fig. 1) [3,1,4]. This finding was supported by histologies showing some gradually distracted specimens exhibited large amounts of

periosteal bone regeneration with little or no cartilage formation (Fig. 3).

A potential limitation of our models is that we have modeled all tissues as linearly elastic, single phase materials for our FE analyses. This material assumption requires input of just two material properties, E and v. Specific to our analyses, this modeling approach is quite appropriate since we are interested in the initial mesenchymal tissue response to the 0.25 mm step distraction, i.e., the time period immediately following distraction when the distraction force reaches its maximum value. During the 0.5 s it takes to apply the 0.25 mm distraction, our experimental data showed that the tissue responds in a linear fashion up to the maximum distraction force [9]. After this initial response, the tissue exhibits a nonlinear stress relaxation response. If we were interested in analyzing the behavior of the tissue during its relaxation period, or at slower loading rates, a poroelastic, biphasic or viscoelastic model would likely be more appropriate. In addition, for the newly forming bone within the distraction gap, we calculated E and v using a linear interpolation of material properties from the mesenchymal tissue stage through the mature bone stage. In the future, as more experimental data on the mechanical properties of immature bone become available, a more accurate constitutive model could be implemented.

The finite element analyses performed here provided information beyond that which we could determine in our previous experimental study. Strains determined empirically provided us with information about the global strain state. The detailed FE analyses developed here were required in order to understand the local strain state and, specifically, why bone regeneration occurred in certain regions of the distraction gap and periosteal to the bone ends and why the amounts of new bone formation varied in specimens from different time points. We were further able to calculate hydrostatic stresses in the complicated geometries, something that we could not do with our empirical analyses.

By performing CT-based finite element analyses at four distinct time points during distraction, we were able to obtain information about tissue regeneration throughout distraction. Other investigators' FE analyses of distraction osteogenesis have been performed at one time point, thus providing information about the mechanical environment for only one specific time during distraction [14–16]. Our FE analyses showed how the patterns and magnitudes of hydrostatic stress and tensile strain change throughout distraction. As a result of this information, we were able to determine that tensile strain magnitudes up to 13% appeared to correspond to new bone formation at all time points (end latency and distraction days 2, 5, and 8). An environment of mild hydrostatic stress might also have contributed to new bone formation as the highest hydrostatic pressure was less than 17 kPa and the highest tensile hydrostatic stress was less than 97 kPa, both values well within the "low" range of hydrostatic stresses required for new bone formation as defined by Claes and Heigele in their experimental and computational work on fracture healing (they found that regions of hydrostatic stress $<\pm 150$ kPa allowed for direct bone formation) [4]. However, a limitation of our approach is our modeling of the regenerate tissue as a near-incompressible single phase solid, which does not account for the fluid in the tissue. A single phase finite element model calculates the net traction causing equilibrium on each plane. An inherent limitation of the method is that it is not possible to directly interpret the net stress onto the components of a multiphasic material such as real tissue. As mentioned above, we found maximum tensile hydrostatic stresses in the tissue to be equal to 97 kPa. In reality, tensile hydrostatic stresses (i.e., negative pressures) greater than 47.07 mmHg (=6.3 kPa), which is the vapor pressure of water at 37 °C, would cause the water in the tissue to boil. This, of course, did not occur in the regenerate tissue during distraction. Results from our single phase model could be interpreted as having the tensile hydrostatic stresses borne by the solid components with the transfer of tensile stresses to the fluid components causing tensile hydrostatic stresses no less than the vapor pressure of the fluid. In a poroelastic or viscoporoelastic model, the hydrostatic tensile stresses would be shared by both the solid and fluid phases.

The use of a CT/FEA methodology as used in this study allows for the determination of local hydrostatic stresses and maximum principal tensile strains in sites of multipotent mesenchymal tissue with complicated geometries and/or boundary conditions. By more accurately modeling these complicated geometries with the use of CT data, we obtain more useful information about the distraction-induced hydrostatic stresses and tensile strains within the tissue regenerate. With this information, we come closer to a means of noninvasively determining the most appropriate distraction osteogenesis procedure for a patient prior to initiating surgery.

Acknowledgement

This work was supported by NIH R01 grant DE13028 and The Oak Foundation to Michael T. Longaker. We would like to thank David Paik, Gary Beaupré, Rob Gardner, and Erik Ranheim for their contributions.

References

[1] Carter D, Beaupré G, Giori N, Helms J. Mechanobiology of skeletal regeneration. Clin Orthop 1998;355(Suppl.):S41–55.

[2] Carter DR. Anisotropic analysis of strain rosette information from cortical bone. J Biomech 1978;11:199–202.
[3] Carter DR, Beaupré GS. Skeletal function and form. Mechanobiology of skeletal development, aging, and regeneration. Cambridge: Cambridge University Press; 2001. p. 161–200.
[4] Claes L, Heigele C. Magnitudes of local stress and strain along bony surfaces predict the course and type of fracture healing 1999; 32:255–66.
[5] Gateno J, Allen M, Teichgraeber J, Messersmith M. An in vitro study of the accuracy of a new protocol for planning distraction osteogenesis of the mandible. J Oral Maxillofac Surg 2000;58(9): 985–91.
[6] Gateno J, Teichgraeber J, Aguilar E. Computer planning for distraction osteogenesis. Plast Reconstr Surg 2000;105(3):873–82.
[7] Kusnoto B, Figueroa A, Polley J. A longitudinal three-dimensional evaluation of the growth pattern in hemifacial microsomia treated by mandibular distraction osteogenesis: a preliminary report. J Craniofac Surg 1999;10(6):480–6.
[8] Loboa E, Beaupré G, Carter D. Mechanobiology of initial pseudoarthrosis formation with oblique fractures. J Orthop Res 2001;19(6):1067–72.
[9] Loboa E, Fang T, Warren S, et al. Mechanobiology of mandibular distraction osteogenesis: experimental analyses with a rat model. Bone 2004;34:336–43.
[10] Paccione M, Mehrara B, Warren S, et al. Rat mandibular distraction osteogenesis: latency, rate, and rhythm determine the adaptive response. J Craniofac Surg 2001;12(2):175–82.
[11] Paik D, Beaulieu C, Jeffrey R, et al. Automated flight path planning for virtual endoscopy. Med Phys 1998;25(5):629–37.
[12] Parker D, Wang K, Taylor C. Image based geometric modeling of the human vasculature in computational hemodynamics. In: Proceedings of the 1999 ASME Summer Bioengineering Meeting, Big Sky, MT, 1999.
[13] Perren S, Cordey J. The concept of interfragmentary strain. In: Uhthoff HK, editor. Current concepts of internal fixation of fractures. New York: Springer-Verlag; 1980.
[14] Remmler D, Olson L, Duke D, et al. Presurgical finite element analysis from routine computed tomography studies for craniofacial distraction: II. An engineering prediction model for gradual correction of asymmetric skull deformities. Plast Reconstr Surg 1998;102(5):1395–404.
[15] Remmler D, Olson L, Ekstrom R, et al. Pre-surgical CT/FEA for craniofacial distraction: I. Methodology, development, and validation of the cranial finite element model. Med Eng Phys 1998;20(8):607–19.
[16] Richards M, Goulet J, Weiss N, et al. Bone regeneration and fracture healing. Experience with distraction osteogenesis model. Clin Orthop 1998;355(Suppl.):S191–204.
[17] Rockwood Jr CA, Green DP, Bucholz RW. Fractures in adults. Philadelphia: Lippincott; 1991.
[18] Rowe NM, Mehrara BJ, Dudziak ME, et al. Rat mandibular distraction osteogenesis: part I. Histologic and radiographic analyses. Plast Reconstr Surg 1998;102:2022–32.
[19] Samchukov M, Cope J, Harper R, Ross J. Biomechanical considerations of mandibular lengthening and widening by gradual distraction using a computer model. J Oral Maxillofac Surg 1998;56(1):51–9.
[20] Santler G, Karcher H, Gaggl A, et al. Advantage of three-dimensional models in intraoral callus distraction. Comput Aided Surg 1998;3(3):99–107.
[21] Schendel S, Heegaard J. A mathematical model for mandibular distraction osteogenesis. J Craniofac Surg 1996;7(6):465–8.
[22] Swennen G, Figueroa A, Schierle H, et al. Maxillary distraction osteogenesis: a two-dimensional mathematical model. J Craniofac Surg 2000;11(4):312–7.